ChemComm

Tuning Metal-Metal Interactions for Cooperative Small Molecule Activation

Journal:	*ChemComm*
Manuscript ID	CC-FEA-11-2020-007721.R1
Article Type:	Feature Article

ARTICLE

Tuning Metal-Metal Interactions for Cooperative Small Molecule Activation

Received 00th January 20xx,
Accepted 00th January 20xx

DOI: 10.1039/x0xx00000x

Qiuran Wang, Sam H. Brooks,† Tianchang Liu,† Neil C. Tomson*

Cluster complexes have attracted interest for decades due to their promise of drawing analogies to metallic surfaces and metalloenzyme active sites, but only recently have chemists started to develop ligand scaffolds that are specifically designed to support multinuclear transition metal cores. Such ligands not only hold multiple metal centers in close proximity but also allow for fine-tuning of their electronic structures and surrounding steric environments. This Feature Article highlights ligand designs that allow for cooperative small molecule activation at cluster complexes, with a particular focus on complexes that contain metal-metal bonds. Two useful ligand-design elements have emerged from this work: a degree of geometric flexibility, which allows for novel small molecule activation modes, and the use of redox-active ligands to provide electronic flexibility to the cluster core. The authors have incorporated these factors into a unique class of dinucleating macrocycles ($^{n}PDI_2$). Redox-active fragments in $^{n}PDI_2$ mimic the weak-overlap covalent bonding that is characteristic of M–M interactions, and aliphatic linkers in the ligand backbone provide geometric flexiblity, allowing for interconversion between a range of geometries as the dinuclear core responds to the requirements of various small molecule substrates. The union of these design elements appears to be a powerful combination for analogizing critical aspects of heterogeneous and metalloenzyme catalysts.

Introduction

The catalytic transformation of small molecules into value-added products has motivated decades of research in molecular transition metal chemistry. A majority of the work in this area has been devoted to the development of mononuclear catalysts, and enormous gains in catalytic performance have been realized by fine-tuning the steric and electronic profiles of supporting ligand environments.[1-6] Such efforts led to the emergence of a variety of molecular catalysts that are used in industrial processes, like the Grubbs catalysts for catalytic olefin metathesis reactions, various cross-coupling catalysts for use in the synthesis of pharmaceuticals, and Ziegler-Natta catalysts for olefin polymerization.

Other areas of industry are replete with heterogeneous catalysts, including many that operate over promoter-modified metallic surfaces. These catalysts find use in a range of applications, including steam reforming of methane, ammonia synthesis, and catalytic converters. In these processes, the activation of small molecules is generally understood to occur between multiple metal centers,[7-10] *i.e. metal atoms work cooperatively to activate small molecule substrates.* This multinuclear approach to small molecule activation is also used in biological systems, which are able to leverage amino acid side chains and inorganic ligands to create multinuclear clusters that are able to mediate multi-electron and multi-proton transformations. Examples include the multicopper oxidases,[11, 12] which activate dioxygen across three copper centers at a metalloenzyme active site, and the Fe-S clusters of the nitrogenase enzymes that mediate the catalytic reduction of N_2 to NH_3 under ambient conditions.[13, 14]

With an interest in modelling these multimetallic activation processes and discovering novel catalysts inspired by industrial/biocatalytic systems, chemists have sought to design molecular complexes that are able to activate small molecules across multiple metal centers.[15, 16] This field has its origins in Muetterties' study of the cluster-surface analogy, which sought to create low-valent, often late-metal, cluster compounds that would mimic the properties of a metallic surface.[17-19] Many of the compounds studied at the time made use of simple carbonyl, hydride, and phosphine ligands.[19-23] Since then, a variety of metallic complexes supported by σ-donating and π-accepting ligands have been reported and studied for small molecule activation chemistry.[24-34] Examples include Bergman's sulfur-atom abstraction reactions by a heterobimetallic $Cp_2Zr(\mu\text{-}N^tBu)IrCp^*$ complex (Cp* = pentamethylcyclopentadienyl),[25] Mankad's bimetallic (^{Dipp}NHC)Cu–FeCp(CO)$_2$ complexes (^{Dipp}NHC = *N*,*N*'-*bis*(2,6-diisopropylphenyl)imidazol-2-ylidene) that perform catalytic photochemical C–H borylation reactions,[31] and Johnson's pentanuclear nickel cluster that abstracts a carbon atom from alkenes.[32] All make use of ligands that are common to mononuclear transition metal chemistry to construct multinuclear complexes with unique reactivity profiles.

P. Roy and Diana T. Vagelos Laboratories, Department of Chemistry, University of Pennsylvania, 231 South 34th Street, Philadelphia, Pennsylvania, 19104, USA. E-mail: tomson@upenn.edu
† These authors contributed equally.

Building on the success of these unsupported M–M bonded complexes, the field has recently turned its considerable capacity for ligand design to the development of scaffolds capable of housing multiple metal centers within close proximity of one another. Ligand design plays a crucial role in the assembly of multimetallic clusters, as both the electronic and the steric properties may impact cluster aggregation and substrate accessibility.[35, 36] We have categorized these ligand design strategies into two primary classes (Fig. 1). The first involves the design of ligands that support the use of an ancillary metal (M_A) as a ligand on an active site metal (M_B).[37-43] In this case, the coordination environment about M_A is saturated, such that the chemistry performed by the bimetallic complex is localized at M_B. This approach has led to an enormous amount of fascinating chemistry, starting with some of the earliest examples of M–M multiple bonds,[27, 42] through the broad use of dirhodium carbenes in organometallic chemistry,[43-46] and on to later work that has provided more rational control over the identities and coordination environments of both M_A and M_B.[37, 47, 48]

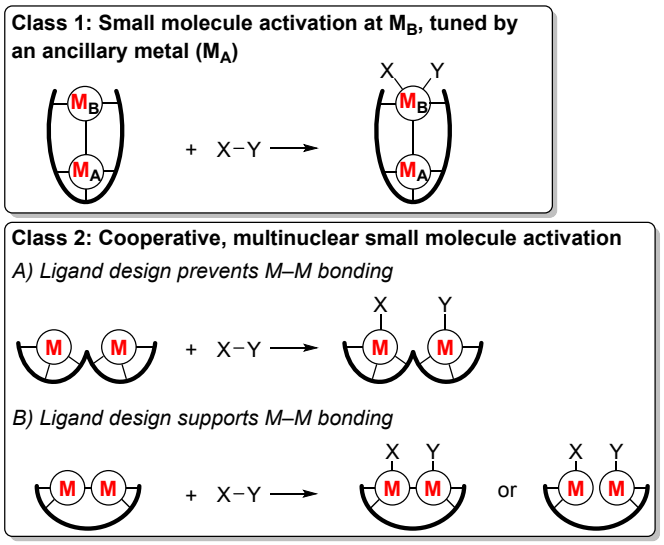

Fig. 1 Categories of ligand design classes aimed at generating multinuclear complexes capable of undergoing small molecule activation chemistry.

The other primary class deals with the design of ligands that allow multiple metal centers to cooperatively bind and activate small molecule substrates. This second approach may be subdivided into systems that hold the metal centers beyond their M–M bonding range (Class 2A) and those that support well-defined M–M bonding (Class 2B). While the former leads to larger binding pockets and typically draws comparisons with bioinorganic active sites, the latter yields high state-densities and is better discussed in the context of both atom-precise clusters and active sites on heterogeneous catalysts. The distinction is important when designing new ligands, since the presence of a M–M bond can be incompatible with many common mononucleating ligands.

This Feature Article is intended to highlight ligand design for multinuclear complexes that appear to undergo cooperative small molecule activation. Following the initial description of a pair of illustrative examples of recent work that falls within Class 2A, the bulk of the text will describe the burgeoning field of ligand design for multinuclear complexes that bear M–M bonds (Class 2B), with a particular focus on the two ligand design criteria that have been critical to our research: i) *limited* geometric flexibility that provides for structural adjustments during small molecule activation and ii) electronic flexibility, which may be used to store and release electron density as needed by the cluster core. Following a survey of past developments in these respective areas, an overview will be presented of our use of a ligand system that merges these concepts to create a system that is able to mimic aspects of metallic surfaces.

Ligand Design for Multinuclear Complexes that Activate Small Molecules

A Case Study in Ligand Design for Class 2A

The scope of chemistry that falls under the heading of Class 2A is too broad to survey here,[49-57] so we will simply illustrate two recent examples of ligand designs that appear to provide a kinetic advantage for small molecule activation by pre-organizing the metal centers with respect to one another. Both examples make use of the classical β-diketiminate (BDI) scaffold, underscoring the breadth of chemistry that is available when even such a well-studied ligand is creatively incorporated into multinucleating platforms.

In the first example, the Meyer group reported a pyrazolate-derived ligand that incorporated BDI groups on the 3- and 5-positions of the pyrazole ring. Deprotonation of this ligand, followed by transmetallation with $NiBr_2$(DME) led to the formation of the dinickel-μ-bromide species **1**. The pyrazolate "linker" between the two metal-ligating BDI units resulted in a long metal-metal distance (3.781(1)Å) and ensured minimal, if any, metal-metal interaction. Upon treatment of **1** with $KHBEt_3$, a dinickel dihydride species **2•K** was formed (Scheme 1).[58] It was found that two aryl rings of the diisopropylphenyl (Dipp) substituents held the K^+ ion through cation–π interactions. The K^+ ion was also found to be coplanar with the pyrazolate-bridged dinickel dihydride core and formed K^+···hydride interactions [d(K^+···H) = 2.45(3)–2.53(3) Å]. Treatment of **2•K** with D_2 revealed the reversible formation of **2-D•K** and H_2 exclusively, without any sign of H/D scrambling. Additional studies indicated that the two Ni–H bonds are formed synchronously.

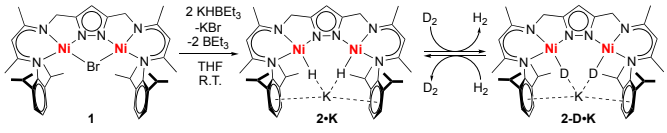

Scheme 1 Reversible transformation between **2•K** and **2-D•K**.

Further studies on the **2•K** complex revealed its ability to behave as a dinickel(I) synthon for reductive binding to small molecule substrates. When treated with small molecules (*e.g.* alkynes, O_2, RN=O, NO), **2•K** was able to lose one molecule of

H_2 and bind the incoming substrate in a μ-η^1:η^1 fashion. In this transformation, the substrate was reduced, and as a result, the corresponding $[RC=CR]^{2-}$,[58] $[O_2]^{2-}$,[59] $[RNO]^{2-}$,[60] and $[N_2O_2]^{2-}$ moieties[61] were generated (Scheme 2). The reduced substrates are then able to undergo further electron- or proton-transfer reactions. The treatment of **2•K** with NO is particularly interesting in that it was proposed to generate an initial transient species with a $[Ni_2(NO)]$ core. It was speculated that the bridging NO unit may bind in an unusual μ-κ^1N:κ^1O-geometry with respect to the Ni centers – similar to the peroxide ligand in **4•K** – before binding an additional equivalent of NO to generate the *cis*-hyponitrite species **6•K**.

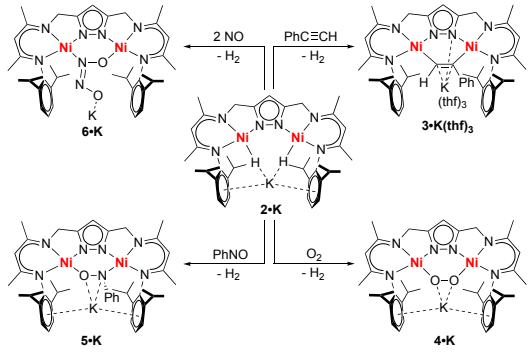

Scheme 2 Selected chemical transformations reported with **2•K**.

It was found that **6•K** would further react with excess NO to form N_2O, with the concomitant formation of the μ-hydroxide complex **7**. Direct treatment of **2•K** with N_2O also led to H_2 loss and the formation of **7**, likely via N_2 release and formation of a basic μ-oxo species that quickly captured a proton from the medium. Treatment of **6•K** with acid generated **7** and N_2O in good yields (Scheme 3). This reactivity is reminiscent of a proposed N_2O formation step from a *cis*-hyponitrite intermediate bound within the flavodiiron nitric oxide reductases (FNORs).[62, 63] The dinucleating ligand scaffold in **6•K** enforces the unique μ-κ^1N:κ^1O *cis*-hyponitrite binding mode, a geometry that appears to be disfavored in related mononuclear systems but may be important to the mechanism of N_2O formation.[64]

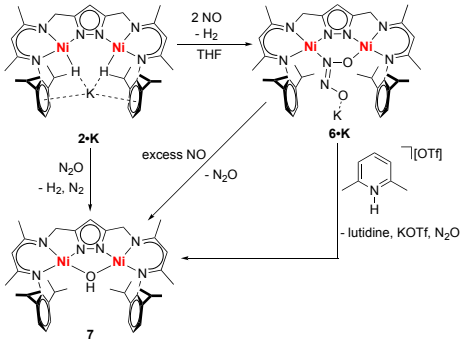

Scheme 3 FNOR-related reactivity enabled by **2•K**.

Recently, Murray and co-workers demonstrated a new design of a cyclophane-based ligand that binds Zn, Cu, Co, Fe, or Mn salts to afford the corresponding trimetallic clusters.[65-68] Within the cavity, the metals are oriented toward each other, each bound by a BDI fragment with no significant metal-metal interactions. The orientation of the three metal centers suggests feasible small molecule activation within the cavity of this cyclophane-based ligand. Deprotonative metallation of this ligand with $[Cu(OTf)]_2{\cdot}C_6H_6$ afforded the first molecular copper(I) dinitrogen complex, **8**, confirming the accessibility of small molecules to the cavity of the cyclophane.[69] Facile displacement of N_2 was achieved in chalcogen (O, S, Se) atom transfer reactions (**9-E**, E = O, S, Se; Scheme 4a).[70, 71] The μ_3-O product **9-O** was also observed upon activation of O_2 by **8**, which exhibited multicopper oxidase-type reactivity.[72]

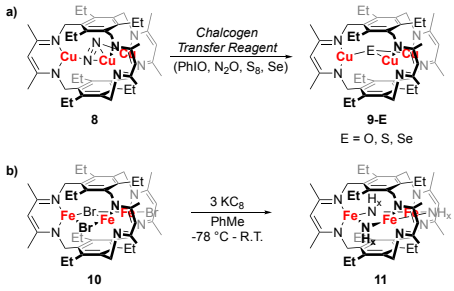

Scheme 4 (a) Chalcogen transfer reactions to the tricopper dinitrogen complex **8**. (b) N_2 activation by the triiron cluster **10** under reducing conditions.

Murray and co-workers also noted the advantage of N_2 accessibility to the cavity through N_2 reduction studies. The triiron cluster, **10** was found to activate N_2 under reducing conditions (Scheme 4b). The formation of triiron amido/imido products were observed, and isotopic labelling experiments confirmed that dinitrogen was being activated.[73] The same bromide cluster was found to be competent for catalytic N_2 silylation (0.2 mol%), affording 50% $N(SiMe_3)_3$ over 96 hours.[74] This chemistry is particularly interesting to consider in light of the Holland group's remarkable demonstration that mononuclear (BDI)Fe complexes are competent for performing the reductive cleavage of N_2 to form a tetrairon dinitride.[75] The inability to isolate a comparable species in the Murray system during N_2 reduction raises the possibility that reaction site tuning offered by the multinucleating cyclophane ligand hinders stabilization of a transient triiron dinitride, but details of the reaction mechanism are still under investigation.[76]

Class 2B: The Importance of Geometric Flexibility

The design of ligands that bind multinuclear complexes and allow for reactivity at a M–M bond presents unique challenges with no clear precedent in traditional and bioinorganic coordination chemistry. The ligands must provide suitable steric protection to the M–M bond, while placing donors in atypical geometries for many organic molecules. In addition, the changes in coordination environments and electronic structures brought by small molecule activation reactions often induce structural rearrangements at the multinuclear core. Several successful examples of ligand design for cluster complexes have leveraged some degree of geometric flexibility in the ligand architecture to promote intermolecular chemistry. The following examples highlight recent work to gain control

over the coordination sphere of M–M bonded cluster compounds. All of the examples described are then shown to make use of the M–M bonded units for small molecule activation chemistry across multiple metal centers.

A three-fold symmetric ligand based on an α-α-α-1,3,5-*tris*-aminocyclohexane scaffold, $[1,3,5\text{-}C_6H_9\text{-}(NPh\text{-}o\text{-}NSi^tBuMe_2)_3]^{6-}$, was designed by Betley and co-workers. This hexaamide ligand provided three dianionic *o*-phenylenediamide subunits for binding multiple metal centers. Complete deprotonation of $[1,3,5\text{-}C_6H_9\text{-}(NPh\text{-}o\text{-}NSi^tBuMe_2)_3]H_6$ with $Fe_2(Mes)_4$ led to trimetallation to form the polynuclear complex **12**.[77] Crystallographic analysis showed an asymmetric binding mode of the hexaamide ligand and an average Fe–Fe distance of 2.577(6) Å, a distance indicative of metal-metal bonding. Cooperative small molecule activation was demonstrated following treatment of **12** with NBu_4N_3. Doing so resulted in reduction of the azide, expelling N_2 and generating the anionic nitrido species, **13** (Scheme 5). Moreover, the ligand reorganized during this transformation to accommodate both the loss of THF and the presence of a bridging nitride. The average Fe–Fe distance contracted in the product to 2.480(1) Å, signifying a higher degree of metal-metal bonding upon oxidation of the trinuclear core.

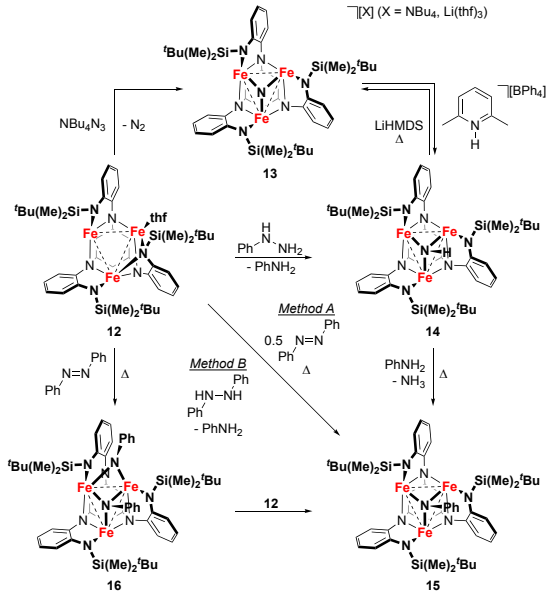

Scheme 5 Activation of the azide ion, hydrazine, and hydrazide derivatives at the triiron core of **12**.

Related studies examined the reducing strength of the cluster in regards to the polynuclear hypothesis, which centers on the combined action of multiple metal centers at both metallic surfaces and metalloenzyme active sites as key for the reduction of dinitrogen to ammonia.[78] This view has found added support recently as attention has turned to a diiron "belt" position as the locus of N_2 activation at nitrogenase active sites.[14] Treatment of **12** with phenyl hydrazine afforded the two-electron oxidized imido complex, **14**, and aniline (Scheme 5). Further heating of this reaction mixture led to the observed transamination products, **15** and ammonia. Key ligand reorganization events were found to accompany these transformations, allowing for the imido moieties to bridge the three iron centers. The use of either diphenylhydrazine or a more oxidized substrate, azobenzene, at room temperature also led to the formation of **15**. It was further found that **12** reacted with azobenzene to first form a *bis*(imido) cluster **16**, which subsequently comproportionated with another molecule of **12** to generate two equivalents of **15**. In total, a four-electron reduction of azobenzene was observed. The reducing nature of the cluster was explained as resulting from both the short metal-metal distances, affording close Fe–Fe bonding interactions, and the electron-rich, strongly donating hexaanionic ligand. Both the two- and four-electron reduction pathways were thus able to be accessed by cooperative activation of the small molecule by the polynuclear cluster.

Thomas and co-workers have targeted the design of heterobimetallic complexes for small molecule activation chemistry. Their work uses untethered phosphinoamide ligands to support clusters composed of early and late first-row transition metals. Much of their work falls under the heading of Class 1 and so will not be described here,[40, 79, 80] but some makes use of the hemilability of the phosphine portion of a ligand to provide access to both metal centers.

For example, the dinitrogen complex **17-N$_2$** has been shown to activate a wide array of small molecules concomitant with ligand isomerization, including electrophiles (MeI, I_2),[81] terminal alkynes,[82] as well as S–H and S–S bonds,[83] carbon-heteroatom π-bonds (ketones,[84] thioketones and imines),[85] and H_2[81] (Scheme 6a). In most instances, activation of the molecule yields a new bridging atom or group following ligand reorganization, an important feature that was also noted by the work of Betley and co-workers.[78] Small molecule activation was similarly demonstrated with *in situ* generated **17**, which was obtained following exposure of **17-N$_2$** to vacuum and contains a stronger metal-metal interaction without dinitrogen acting as a π-acidic ligand. Exposure of **17** to CO_2 led to cooperative deoxygenation of CO_2 (Scheme 6b).[86] The product, **24**, was confirmed by X-ray crystallography and depicts C–O bond cleavage by the metal-metal bond, accompanied by ligand reorganization to yield a less sterically-encumbered position for the bridging oxygen atom. The Thomas group also reported a [TiCo] heterobimetallic complex, which is isostructural to **17** and able to mediate catalytic N–N bond cleavage of hydrazine to form N_2 and NH_3.[87]

The Thomas group has also designed less coordinatively saturated systems. Like their 3-fold symmetric congeners, the heterobimetallic complexes **25**[88] and ^{PR3}**27** (PR_3 = PMe_3, $PMePh_2$)[89] were found to exhibit strong metal-metal interactions through the d_{z2} σ-bonding interaction and dative d_{xz}/d_{yz} π-bonds (Fig. 2). The TiCo heterobimetallic complex **25** highlighted the importance of available coordination sites, as the complex was able to promote the reductive coupling of ketones to form alkenes, as aided by the cleavage of the C–O bond across the Ti≡Co bond.[88] Concomitant metal-oxo cluster (**26**) formation was observed in the presence of NaI, a necessary stoichiometric additive used to obtain the alkene product in good yields over short reaction times (Scheme 6c).

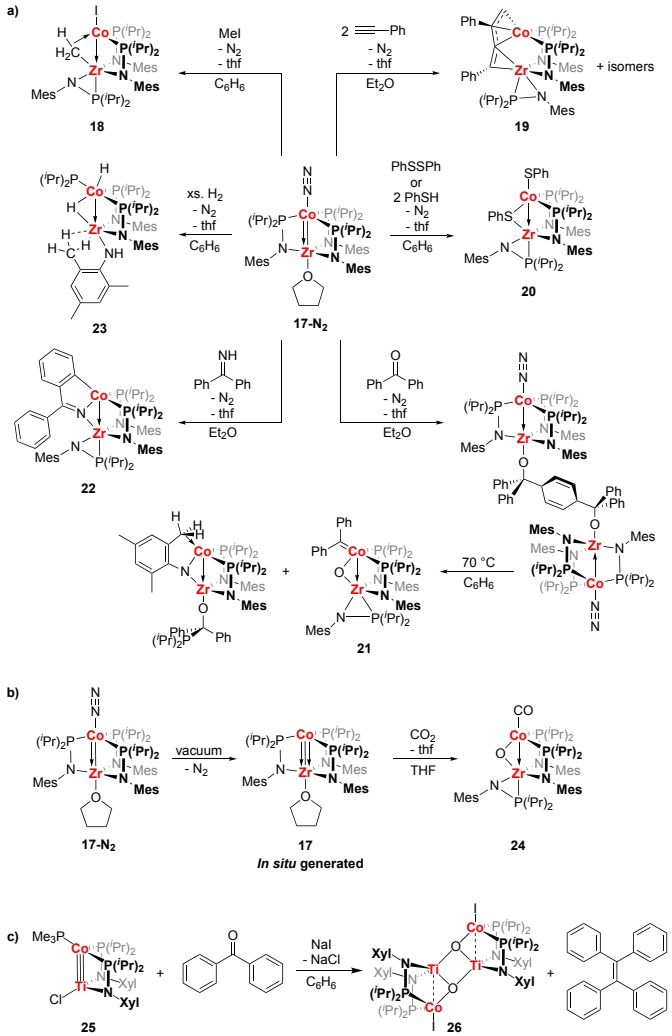

Scheme 6 (a) Small molecule activation by **17-N_2**. (b): CO_2 activation by in situ generated **17**. (c) Reductive coupling of ketones mediated by **25**.

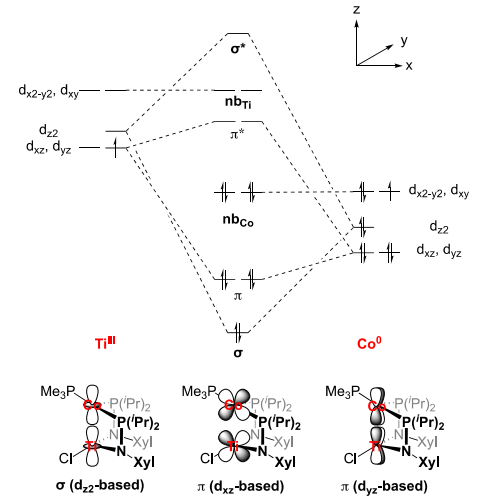

Fig. 2 Representative example of the molecular frontier orbital diagram of **25**.

Likewise, the ZrCo heterobimetallic systems were also found to be active for alkene and alkyne hydrogenation. Exposure of ^{PR3}**27** to an atmosphere of H_2 led to the dihydride product, ^{PR3}**28**, that appears to result from the activation of H_2 across the Zr–Co bond (Scheme 7a).[89] This stoichiometric reactivity prompted catalytic hydrogenation studies. The treatment of ^{PR3}**27** with styrene and H_2 afforded ethylbenzene.[89] The lability of the bound PR_3 group is important, as the alkene must first displace the phosphine before hydrogenation takes place. Thus, the $PMePh_2$-coordinated complex ^{PMe2Ph}**27** was found to be a more active catalyst due to its greater lability (Scheme 7b).

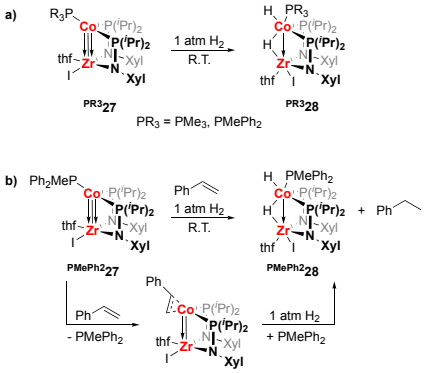

Scheme 7 (a) Activation of H_2 across the Co–Zr multiple bond in ^{PR3}**27**. (b) Hydrogenation reaction of styrene mediated by ^{PMePh2}**27**.

Class 2B: Dinucleating Platforms with Redox-Active Components

In the past decade, redox-active ligands have been shown to play important roles in various catalytic reactions.[90, 91] The valence orbitals of redox-active ligands lie close in energy to the metal d-manifold, but the two are only able to form weak-overlap covalent bonds. This increases the density of states available to the system and decreases the interelectron repulsion between the electrons that occupy these covalent orbitals. As a result, redox events at complexes that bear such ligands allow for significant contributions from the ligand when undergoing redox processes that would traditionally occur at a metal center. This allows redox-active ligands to work as reservoirs of electrons/holes for a variety of catalytic reactions, thus mimicking the electron delocalization that occurs as a result of M–M bond. In this way, redox-active ligands can be thought to extend the nuclearity of a cluster complex. This section will highlight the use of known redox-active ligands to support multinuclear complexes with close M–M distances.

Metal-arene interactions have been found to afford stabilization of low-valent intermediates in catalytic processes,[92, 93] and the observation that multiple metal centers can coordinate to a single arene scaffold has spurred interest in ligand design to support M–M bonded clusters. The Agapie group has reported the synthesis of a *p*-terphenyl diphosphine ligand. Treatment of this ligand with 1.0 equiv. of $Ni(COD)_2$ and 1.0 equiv. of $NiCl_2$(dme) resulted in a comproportionation reaction, affording a dinuclear Ni^{I} complex, **29** (Scheme 8).[94] Crystallographic analysis revealed significant bonding interactions between the two nickel centers ($d_{Ni–Ni}$ = 2.36580(16) Å) and the central aryl ring of the terphenyl unit ($d_{Ni–Ct(C2)}$ = 1.952 Å and 1.953 Å, respectively; Ct = centroid). In one application of this system, it was found that treatment of **29** with the di-Grignard reagent *o*,*o*'-biphenyldiyl magnesium bromide afforded the corresponding biphenyldiyl complex **30**.

Subsequent treatment with dichloroalkanes yielded fluorene, while treatment with CO led to CO insertion to generate fluorenone (Scheme 8). This reactivity highlights the ability of these systems to undergo dinuclear redox transformations relevant to organic methodology.

It is interesting to note that each of the nickel centers in **30** is coordinated in an η^3 fashion with the central ligand phenyl ring. This phenyl ring is found to be significantly distorted towards a boat conformation, which was not observed in the precursor **29**. The distortion of the arene ring may be an indication of the redox noninnocence between the dinickel core and the π* system of the arene,[95] as has been described in more detail by Agapie in related work on mononuclear Mo chemistry.[96-98] This concept of ligand-based redox activity will return in several examples described below.

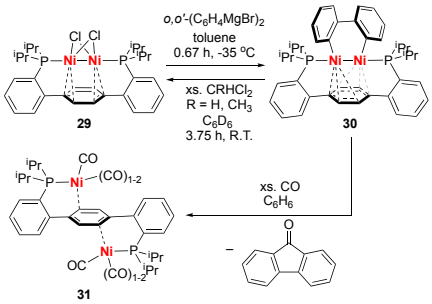

Scheme 8 Chemical transformations on the dinickel platform of **29**

The 1,8-diazanaphthalene unit (naphthyridine) is quickly adopting what may be considered a role as a "privileged"-ligand in dinuclear chemistry. The 1,8-positioning of the nitrogens is similar to other "A-frame"-type ligands (acetates, amidinates, etc.) that have been used for decades in paddlewheel complexes.[99] But the ability to build scaffolding onto the 2,7-positions makes these organic fragments ideally suited for binding and stabilizing a variety of bimetallic cores. [100-107] As will be shown later, these backbones can undergo redox non-innocence when imino groups are bound in the 2,7 positions, but first, we will describe the structural rigidity offered by the napthyridine backbone and the use of napthyridines in chemically non-innocent "expanded pincer" ligands.

The Tilley group installed a $-CR(2\text{-pyr})_2$ arm (R = F or CH_3) at the 2- and 7-positions of a naphthyridine moiety and formed the DPEN (R = CH_3, 2,7-*bis*(1,1-di(2-pyridyl)ethyl)-1,8-naphthyridine) or DPFN (R = F, 2,7-*bis*(fluoro-di(2-pyridyl)methyl)-1,8-naphthyridine) ligands.[108, 109] The DPEN and DPFN ligands were shown to be able to hold two metal cations in close proximity and support bimetallic complexes consisting of different metal centers.[108-110] In particular, the DPEN ligand is able to hold two Cu^I centers in close proximity to bind a variety of two-electron donors (MeCN, XylNC, and CO) in a $\mu\text{-}\eta^1\text{:}\eta^1$-fashion. [108] Computational studies suggest that the short distances between the copper centers (< 2.5 Å) are best assigned as closed-shell cuprophilic interactions. Each copper center provides an empty, angled σ-type orbital originating from its 4s and 4p manifolds. The two empty orbitals from the two copper centers interact cooperatively with the donor orbital on the central ligand to form 3-center, 2-electron (3c,2e) bonds (Fig. 3a). Further studies on this system revealed that the DPFN ligand can support a Cu^I_2 center that is capable of binding C≡P and C≡C bonds in a $\mu\text{-}\eta_2\text{:}\eta_2$-fashion, where the substrate→Cu_2 interaction mainly involves donation from the occupied π-orbitals of the triple bond to the empty 4s orbital on each copper center (Fig. 3b).[111]

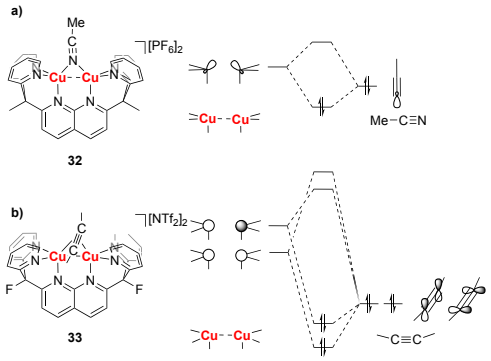

Fig. 3. Orbital diagram showing (a) the (3c, 2e) bond between acetonitrile and the Cu_2 core in **32**, (b) the substrate→Cu_2 donating interaction in **33**.

The DPFN-supported dicopper complex **34** was later found to react with tetraarylborate anions BAr_4^- (Ar = C_6H_5, C_6F_5, and 3,5-$(CF_3)_2$-C_6H_3) and mediate aryl group transfer reactions onto the Cu^I_2 core to form a bridging aryl complex. In particular, treatment of **34** with 1 equiv. of $NaBPh_4$ yielded the bridging phenyl complex **35** (Scheme 9a).[109] These Cu^I_2 bridging aryl complexes were found to undergo one electron oxidation to afford mixed-valent Cu^ICu^{II} bridging aryl complexes, in which the spin density is localized on one copper center instead of delocalized on the bimetallic core, according to EPR, UV-Vis-NIR spectroscopic data and computational studies. **35** is also capable of facilitating C–H activation processes at high temperatures. Treatment of **35** with *p*-tolylacetylene at 100 °C afforded the corresponding bridging *p*-tolylacetylide species **36** (Scheme 9a).[112] The latter was able to mediate the cycloaddition reaction of *p*-tolylazide on the bridging *p*-tolylacetylide moiety and yield a bridging triazolide species **37** (Scheme 9b). Treatment of **37** with *p*-tolylacetylene at room temperature yielded **36** and 1,4-*bis*(4-tolyl)-1,2,3-triazole. This unique reactivity profile prompted the use of **36** as a catalyst (10 mol % loading) in the same azide-alkyne cycloaddition reaction (90% yield after 5.3 h at 100 °C).

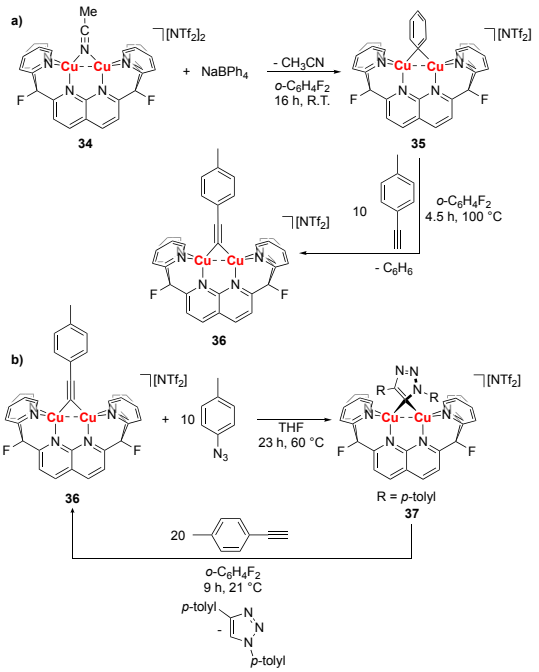

Scheme 9 (a) Aryl transfer reactions to **34** to form **35** and subsequent C–H activation to form **36**. (b) Alkyne-azide cycloaddition reaction mediated by **36**.

Another example of a dicopper system supported by a napthyridine framework was reported by the Broere group, who used an "expanded pincer" ligand, ($^{t\text{Bu}}$PNNP)H_2 that was formed by installation of –$CH_2P^tBu_2$ groups at the 2- and 7-positions of the naphthyridine ring.[113] This ligand was shown to undergo two stepwise, reversible deprotonation processes accompanied by naphthyridine dearomatization to form [($^{t\text{Bu}}$PNNP)H]$^-$ (mono-deprotonated) and [($^{t\text{Bu}}$PNNP)]$^{2-}$ (doubly deprotonated)

Dinuclear Cu^I species were produced by treatment of ($^{t\text{Bu}}$PNNP)H_2 with 2.0 equiv. of Cu^I salts. When mesitylcopper was used as the Cu^I source, a dicopper bridging mesityl complex could be formed. The protonation state of the ligand was shown to affect the bonding of the μ-mesityl group in the [Cu_2(μ-mesityl)] core in this complex.[114] In particular, the ligand's transition from one protonation state to the other could be used to activate hydrogen-containing species. Upon treatment of the bridging *tert*-butoxide species **39** with H_2, dihydrogen was *cooperatively* activated by the dicopper center and the [($^{t\text{Bu}}$PNNP)]$^{2-}$ ligand to form **40** with a "butterfly-shaped" [$Cu_4(\mu_3\text{-H})_2$] core supported by two [($^{t\text{Bu}}$PNNP)H]$^-$ ligands (Scheme 10).[113] The cooperativity between the bimetallic core and the ligand was supported by isotopic labelling experiments, in which the use of D_2 instead of H_2 resulted in deuterium incorporation into both the μ_3-*H* position as well as the ligand C*H*$_2$P^{t}Bu$_2$ and C*H*P^{t}Bu$_2$ backbone. However, treatment of **40** with D_2 at 40 °C, with or without KO^{t}Bu present, did not lead to such deuterium incorporation reactivity, indicating that H_2 activation across the dicopper core and the ligand is reversible and occurs before the formation of **40**.

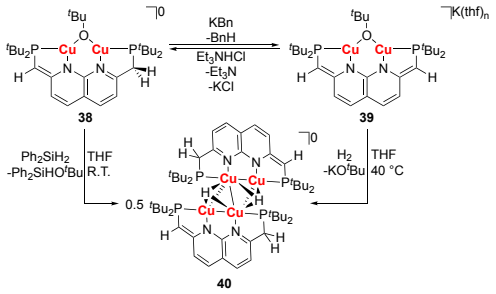

Scheme 10 H_2 activation by **39**.

The Uyeda group was first to report the use of the redox-activity of the naphthyridinediimine (NDI) ligand. The complexation of the neutral ligand with two equivalents of Ni^0 caused the NDI ligand to be reduced by two electrons, while the two Ni^0 centers were oxidized. The two Ni^I centers formed a Ni–Ni bond and bound benzene to generate product **41** (Scheme 11a).[115] The [(NDI)Ni_2] moiety in **41** was shown to traverse 5 different charge states by cyclic voltammetry. Isolation, characterization, and computational studies on the corresponding complexes support that the ligand exists in oxidation states of -2, -1 and 0, while the [Ni_2] core adopts charges of +1 to +3. Treatment of **41** with allyl chloride resulted in a dinuclear oxidative addition reaction to afford a dinickel allyl complex **42**, in which the allyl anion forms a symmetric η^2-1,3-κ^2-interaction with the dinickel core (Scheme 11a).[116] Computational studies suggest that the Ni centers retain +1 oxidation states in this reaction, which indicates that the NDI ligand provides the electron density needed for the activation of allyl chloride.

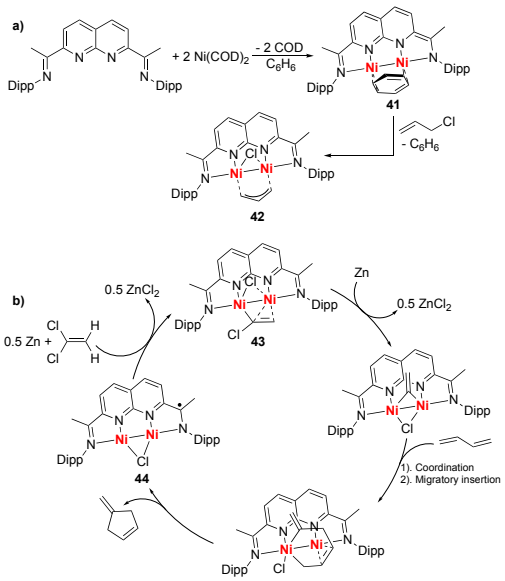

Scheme 11 (a) Formation of the dinickel complex **41** and its allyl chloride activation. (b) Proposed catalytic cycle of the [4+1] cycloaddition reaction catalyzed by [(NDI)Ni_2]-based complexes

Complex **41** has also been used to activate CH_2Cl_2 and mediate catalytic reductive cyclopropanation reactions.[117] Mono-nickel complexes with structurally similar chelating ligands do not show similar catalytic performance. These

control reactions illustrate the crucial role of the dinickel core in the catalytic performance. Later studies revealed that NDI-bound dinickel complexes are also capable of activating vinylidene chlorides *en route* to the catalytic reductive vinylidene transfer to C=C bonds. This chemistry forms either methylene cyclopropane derivatives[118] or, when 1,3-dienes are used as substrates, [4+1] cycloaddition products (Scheme 11b).[119, 120] An important intermediate in the catalytic cycle is proposed to be a [(NDI)Ni_2(η^2-ClC=CH_2)(μ-Cl)] species (**43**) that is formed by oxidative addition of vinylidene chlorides on the bridging chloride species **44**, followed by reduction and halide abstraction by 0.5 equiv. of Zn. The presence of this complex is supported by the isolation of **45**, which was formed from the oxidative addition of BrCH=CHPh to **41** (Scheme 12). The lack of a second halide prohibited further C–X activation of the substrate.[118]

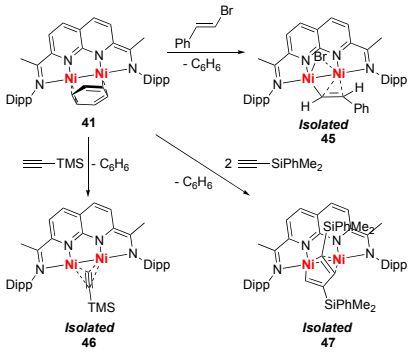

Scheme 12 Formation of important intermediates in catalytic organic transformations catalyzed by NDI-bound dinickel complexes.

Aside from the dinuclear oxidative addition of C–Cl bonds, the (NDI)Ni_2 moiety was also found to mediate a wide variety of chemical transformations[121-128] and, in particular, coordinate and activate unsaturated C–C bonds as parts of catalytic ring formation/rearrangement reactions.[129, 130] **41** was reported as an effective catalyst towards alkyne cyclotrimerzation reactions with 1,2,4-trisubstituted benzenes as the major products, while structurally similar mono-nickel complexes showed poorer reactivity.[130] The key intermediates in this dinickel-facilitated ring-formation reaction were identified by the isolation of **46** and **47** by using trimethylsilylacetylene and phenyldimethylsilylacetylene as the substrates, respectively (Scheme 12). The former compound can be viewed as the first species formed *en route* to the alkyne cyclotrimerized product. The substrate in this complex is coordinated to the dinickel center in a (μ-η^2:η^2) fashion, and a significant elongation of the C≡C bond was observed. **47** represents the active metallocyclic species formed when a second equivalent of alkyne enters the catalytic cycle. Only one Ni is included in the five-membered metallocycle, while the other Ni provides stabilization to the metallacyclopentadiene system via a dihaptic π-interaction with one of the double bonds. This dinuclear stabilization is similar to those proposed in $Co_2(CO)_8$-catalyzed Pauson-Khand reactions.[131, 132]

Combining Redox-Active Fragments with Geometric Flexibility

Our group has been working with a series of dinucleating macrocyclic ligands that offer two primary points of interest with respect to small molecule activation chemistry. One is the inclusion of redox-active elements as a way to expand the electronic flexibility of the cluster core. This is achieved by use of two pyridinediimine (PDI) units, which are well-known redox-active ligands for mononuclear coordination complexes.[133, 134] The second is an element of geometric flexibility, included in this present case by way of catenated methylene linkers that join the PDI imino nitrogens. Both elements find precedent in the examples highlighted above. The electronic flexibility of Uyeda's complexes, for instance, provides access to rich redox chemistry at a robust dinickel core, and the comparison between the Murray and Holland complexes (see above) illustrates the potential impact of altering control over the positions of the metals. This latter point also finds support from the field of heterogeneous catalysis. Metallic surfaces are known to undergo restructuring during substrate binding, activation, and transformation into the products.[135] It is thought that this *limited* mobility of the metal atoms at the surface is important both for providing stabilization to the range of surface species that develop through the course of the reaction and for avoiding entry into thermodynamic sinks.

Drew, Nelson, Nelson, and co-workers first reported a series of bimetallic first-row transition metal complexes supported by a series of macrocyclic ligands that contain two 2,6-diiminopyridine (PDI) units, linked at their imino nitrogens by catenated methylene linkers (e.g. –$CH_2CH_2CH_2$–).[136-140] However, reactivity studies of these complexes were limited due to poor solubility in common organic solvents.[137] We recently revisited this ligand and found that upon installation of *tert*-butyl groups at the 4-positions of the PDI moieties, the solubility profiles of the resulting complexes increased significantly. This minor synthetic modification provided access to a range of reduction chemistry, allowing for further study into the electronic structures of these complexes and their reactivity toward small molecules. This modified ligand is noted as $^nPDI_2$ in the following text, where n is the number of catenated CH_2 units between the two PDI groups.

Recently we reported a series of diiron complexes in which we observed the interconversion of two different conformations of the ligand – "stair-step" and "folded".[141] The THF-soluble diiron complex **48** rests in the stair-step conformation (Scheme 13), in which the Fe_2(μ-Cl)$_2$ core constitutes an edge-sharing connection between two octahedral metal centers. The planes of the PDI units in **48** are roughly parallel to one another, with the pyridyl nitrogens facing in opposite directions. Upon either anion metathesis to form **49** or reduction to form **50**, the ligand was found to adopt a folded conformation, in which the planes of the PDI units were again found to be roughly parallel but the pyridyl nitrogens pointed in the same direction. Reduction of **49** or salt metathesis of **50** with NaSPh both led to the ligand reverting to a stair-step conformation on formation of a [Fe_2(μ-SPh)$_2$] core.

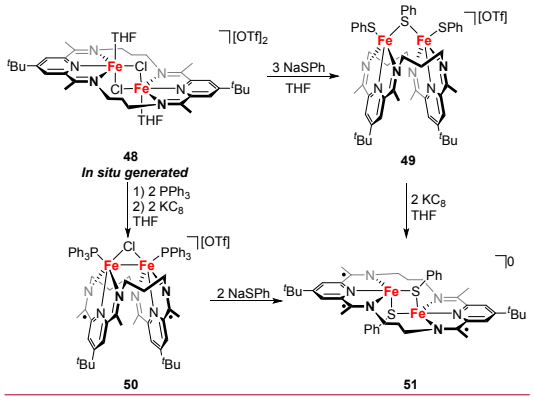

Scheme 13 Ligand conformation change in the series of diiron complexes. Adapted with permission from reference 141. Copyright 2019 American Chemical Society.

We also observed that the ligand's geometric flexibility extends to an ability to hold the metal centers in a wide range of M–M distances. X-ray crystallographic studies revealed an Fe–Fe distance of 3.3262(5) Å in **48** and 2.7320(11) Å in **51**. Both display the stair-step ligand geometry but exhibit a ~0.6 Å difference in Fe–Fe distances. More recently, we reported the synthesis and characterization of a series of bimetallic iron, cobalt and nickel complexes **52** - **57** that are isostructural to the folded-ligand complex **50** (Fig. 4).[142] Inspection of their crystallographic data also revealed a wide range of metal–metal distances (Fig. 4) that again spanned nearly 0.6 Å, from 2.63-3.22 Å.

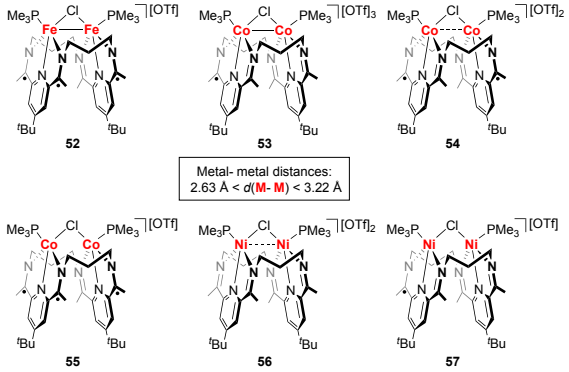

Fig. 4 Molecular structures of bimetallic iron, cobalt and nickel complexes **52** – **57** supported by the ^{3}PDI$_2$ ligand.

In addition to exploring the variety of geometric structures supported by the ^{3}PDI$_2$ ligand, we have been interested in determining the electronic structures of these complexes as a way of guiding our understanding of the small molecule activation chemistry described below. In the folded complex **49**, variable temperature XRD studies revealed that the ligand maintains the [Fe$_2$(SPh)$_3$] core in a folded conformation despite the increase in Fe–Fe distances from 3.1726(5) Å at 100 K to 3.2344(8) Å at 250 K (Fig. 5).[141] These data were correlated through SQUID magnetometry and DFT studies to the presence of a wide range of thermally accessible spin states, ranging from the diamagnetic ground state up through an S = 8 state. The magnetic states were found to result from population of Fe–Fe antibonding orbitals, leading to the cleavage of the Fe–Fe bonding interaction on warming.

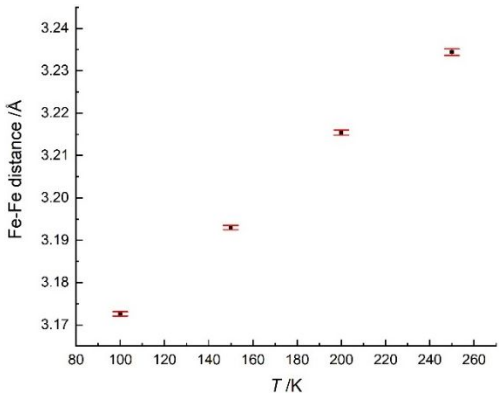

Fig. 5 Fe–Fe distances in **49** at different temperatures. Error is depicted as red bars. Reprinted with permission from reference 141. Copyright 2019 American Chemical Society.

Complexes **52** - **57** constituted a *pseudo*-electron transfer series that allowed for an in-depth investigation into the interdependence of the M–M bonding and the extent of ligand reduction.[142] Two metrics in particular have been useful for delineating the trends in the experimental data. One is the imputed M–M bond orders as determined by their formal shortness ratios (FSRs),[143] which are equal to the intermetallic distance divided by the sum of the single bond covalent radii of the metal centers.[144] The other is the physical oxidation state of the ligand (Δ_{avg}, average Δ value[134] for the two PDI moieties on the ligand; Table 1). The Δ value represents the difference between the average C–N and C_{im}–C_{py} distances on the ligand backbone. These FSR and Δ_{avg} data for the bimetallic complexes are given in Table 2, and the combination of these values with computational studies suggested significant mixing of ligand π^* character and M–M bonding/antibonding character in the valence region of these compounds (Fig. 6). When these valence orbitals are populated, electron density will be transferred to both the M–M σ-(anti)bonding and ligand π^* manifolds. As such, the population of electrons in these orbitals affects both M–M bond orders and the ligand oxidation states. As will be described below, the covalency in the M–PDI interactions was also calculated to play a role in the electronic structure of an N_2-bound diiron species.

Table 1 Δ_{avg} values of $^{3}PDI_2$ ligands in different oxidation states. Adapted with permission from reference 142 (https://pubs.acs.org/doi/10.1021/acs.inorgchem.9b02339). Copyright 2020 American Chemical Society. Further permissions related to the material excerpted should be directed to the ACS.

$^{3}PDI_2$ oxidation state	Δ_{avg} /Å
$(^{3}PDI_2)^{0}$	0.171
$(^{3}PDI_2)^{-}$	0.138
$(^{3}PDI_2)^{2-}$	0.104
$(^{3}PDI_2)^{3-}$	0.080
$(^{3}PDI_2)^{4-}$	0.056

Table 2 FSR values and Δ_{avg} values of complexes **52** – **57**. Adapted with permission from reference 142 (https://pubs.acs.org/doi/10.1021/acs.inorgchem.9b02339). Copyright 2020 American Chemical Society. Further permissions related to the material excerpted should be directed to the ACS.

	52	**53**	**54**	**55**	**56**	**57**
Δ_{avg} /Å	0.086	0.134	0.119	0.085	0.163	0.138
FSR	1.138	1.138	1.207	1.349	1.181	1.397

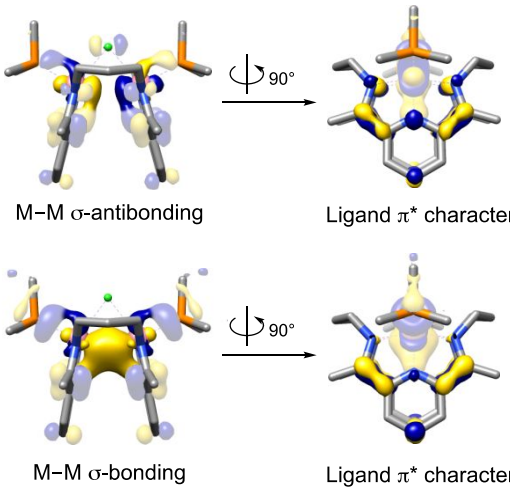

Fig. 6. Selected example showing mixing of M–M bonding/antibonding character with ligand π* character in selected molecular orbitals of complexes **52** - **57**.

Further reactivity studies on $^{n}PDI_2$-supported bimetallic complexes revealed their ability to activate substrates in a bimetallic fashion. Reduction of **50** or **52** with 2.0 equiv. of KC_8 resulted in the formation of diiron-μ-N_2 complexes ^{PR3}**58** (PR_3 = PMe_3, PPh_3) with unusual Fe-Ct_{N2}-Fe angles of *ca.* 150° (Ct_{N2} = centroid of N_2; Scheme 14, Fig. 7a).[145] These Fe-N_2-Fe geometries are highly unusual for molecular μ-N_2 complexes,[146, 147] as most form linear bridges that maximize π-backbonding from the traditional d_π orbitals into the N_2 π*-manifold. The geometry is reminiscent, however, of the α-N_2 binding mode on Fe(111) surfaces[148] – a critical binding mode that precedes N_2 cleavage during the catalytic reduction of N_2 to NH_3 in the Haber-Bosch Process. The bridging N_2 units in ^{PR3}**58** are mildly activated (N–N = 1.135(3) for PR_3 = PMe_3 and 1.139(3) Å for PR_3 = PPh_3), consistent with the spectroscopically observed N–N stretching frequencies of 2003 and 1959 cm^{-1}, respectively.

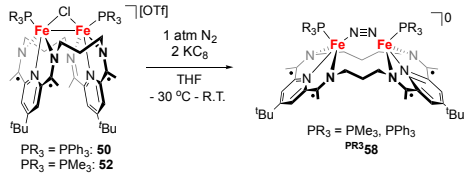

Scheme 14. Synthesis of the bridging N_2 complex ^{PR3}**58** from **50** and **52**.

The unusual N_2 binding geometries in ^{PR3}**58** appear to result from the constraints imposed by the macrocycle, as the ligand is unable to unfurl far enough to support a linear Fe–N_2–Fe geometry. This may be compared to the other known examples of similar Fe–N_2–Fe geometries, which feature alkali metal ions in proximity to the μ-N_2 units. Holland reported the example of $Fe_3(\mu\text{-}N_2)_x(\mu\text{-}Cl)_{3-x}$ rings (x = 2, 3) capped by alkali metal ions,[146] and Mindiola reported the use of two meridonally coordinated Fe centers linked through K-arene interactions in addition to the μ-N_2 unit.[147] It is unclear in these systems whether the alkali metals are ancillary counterions, necessary components for generating constrained geometry macrocycles, or partners in tuning electronically driven geometric features. But given the structures the α-N_2 binding mode on Fe(111) and the discovery of related μ-κ^1N:κ^1N geometries at the active-site belt positions of a reductant-depleted nitrogenase,[14, 148] we were interested to determine the electronic structure changes that result from this unusual binding geometry.

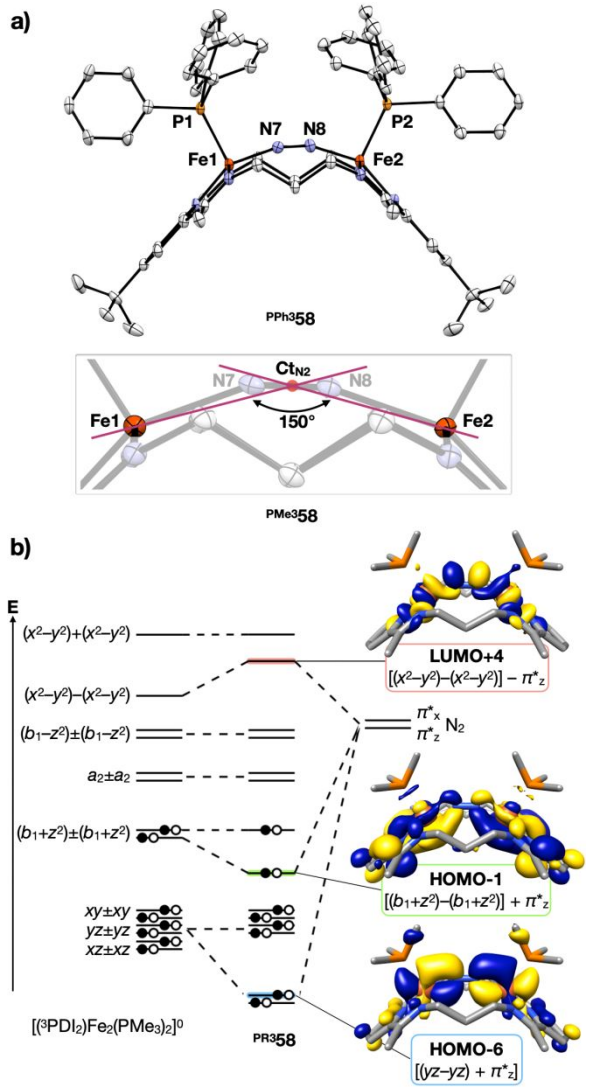

Fig. 7. Crystal structure (a) and electronic structure (b) of ^{PR3}**58**. Adapted with permission from reference 145. Copyright 2020 American Chemical Society.

Despite the modest activation of N_2 in ^{PR3}**58**, computational studies revealed interesting orbital interactions that may be of use to the field. In addition to the traditional π-backbonding interactions (e.g. HOMO-6), HOMO-1 was found to result from admixture of $^3PDI_2$ π* character into the N_2 π* manifold, as mediated by the Fe d_{z2} orbitals. To higher energies, the LUMO+4 was identified as resulting from backbonding of Fe d_{x2-y2} – a d_σ orbital – into the N_2 π* system (Fig. 7b). This unusual π-backbonding interaction has implications for the mode of N_2 activation at other constrained geometry binding sites, especially those with high-spin electron configurations at Fe.

Small molecule activation was also discovered for a $^3PDI_2$-bound dicobalt system. Reduction of the **55** by 1.0 equiv of KC_8 in the presence of 0.5 equiv of MeCN led to C–C bond activation of MeCN and the formation of equimolar amounts of a bridging methyl complex **59** and bridging cyanide complex **60** (Scheme 15).[149] The former complex is the first structurally characterized example of a bridging methyl group on Co. An agostic interaction was apparent from the ^{1}H NMR spectrum, which revealed inequivalence (2H:1H) of the methyl hydrogens at low temperatures with the 1H signal displaying an upfield signal (-12.7 ppm) with a small C–H coupling constant ($^1J_{CH}$ = 74.5 Hz). In the latter complex, **60**, the [C ≡ N]$^-$ unit bridges between the Co centers in a μ-CN-κ^1C:κ^1N fashion, reminiscent of the N_2 binding mode in the isoelectronic ^{PR3}**58** species. Upon one-electron oxidation of this complex, a weak Co–Co bond is formed, and as a result, the binding mode of the [C ≡ N]$^-$ unit changed to a μ-CN-κ^1C:η^2-CN fashion (Scheme 15). This is an atypical, semi-bridging configuration that has not been reported previously for Co. Notably, the ligand geometry changed from arched to folded to allow for closer contact between cobalt atoms, highlighting both the geometric flexibility of the ligand scaffold to enable the cleavage and reformation of M–M bonds and the access to unique small molecule binding modes as a result of the macrocyclic framework.

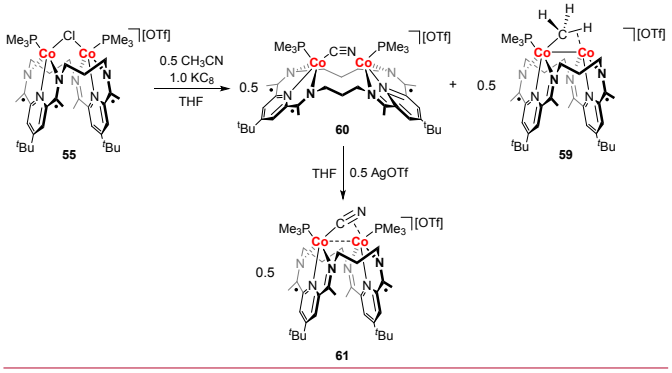

Scheme 15 MeCN activation and C≡N binding mode change on the [$^3PDI_2$-Co_2] platform.

Aside from reduction of the bridging chloride complexes, interesting reactivity was also observed on substitution of the bridging chloride with an azide. Treatment of **52** with NaN_3 resulted in the formation of a diiron bridging nitride species **62** (Scheme 16).[150] Crystallographic studies revealed a change in the $^3PDI_2$ ligand conformation from folded to stair-step to accommodate the linear Fe-N-Fe moiety. The Fe-N_μ bond distances of 1.677(3) and 1.673(3) Å indicate multiple bond character similar to what has been reported for Fe imido complexes,[151, 152] and the Δ_{avg} value of 0.073 Å is indicative of a $(^3PDI_2)^{3-}$ ligand.

Considering that bridging iron nitrides serve as key intermediates in catalytic ammonia synthesis, we are delighted to find that **62** presents a diverse profile of N–H bond formation chemistry. Treatment of **62** with Ph_2PH led to the clean formation of a diamagnetic bridging amide species **63**, concomitant with the formation of an equivalent of Ph_2P–PPh_2, suggesting two PCET reactions from the phosphine to the nitride center (Scheme 16). During this reaction, the ligand was found to have folded to support the change from an *sp*-hybridized μ-N to an *sp*^{3}-hybridized μ-NH_2 unit. Moreover, **62** was also found to react with $PhSiH_3$ and HBpin (pin = pinacolate) to generate the E–H insertion products, ^{NHE}**64** (NHE = NHBPin, $NHSiH_2Ph$). Finally, treating **62** with 3.0 equiv. of PhSH was found to completely remove the μ-N moiety and form NH_3 in 71% yield. The product from this reaction, **49**, reveals oxidation

of the $(^3PDI_2)^{3-}$ in **62** to $(^3PDI_2)^0$ in **49**, consistent with an intramolecular electron transfer in addition to N–H bond formation.

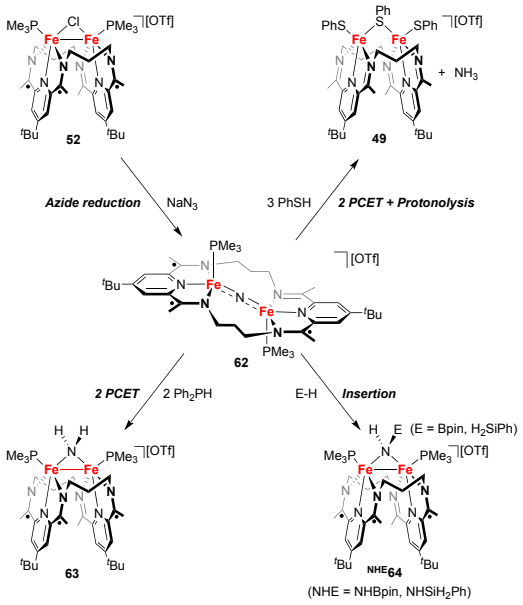

Scheme 16 Chemical transformations mediated by **62**.

We were unable to isolate a bridging azide species by salt metathesis of **52** with NaN_3. However, treatment of its isoelectronic dicobalt congener **53** with NaN_3 led to the isolation of a dicobalt bridging azide species **65** (Scheme 17).[153] The complex displayed a folded ligand geometry with unusually short Co–N distances of *ca*. 1.94 Å. Despite the Co(II) physical oxidation state of each Co ion, the phosphines were found via NMR spectroscopy (EXSY) to be inert with respect to exchange, presumably as a result of the Co–Co bonding interaction (2.5819(4) Å) *trans* to the phosphine.

Thermolysis of **65** resulted in the isolation of products that are consistent with the transient formation of a dicobalt nitride – a moiety that was unknown to the field at the time.[154] Heating **65** at 60 °C in MeCN led to the formation of an amide species **66** in low, albeit reliable, yields. This result was consistent with an initial thermolysis of the azide, followed by the abstraction of two hydrogen atoms from an unknown source. The yield of **66** was increased by heating the complex under 1 atm of H_2 (Scheme 17). However, performing the same reaction with D_2 resulted in deuterium incorporation on the ligand CH_2 linkers, with no detectable D-incorporation at the amido group. This isotopic labelling experiment indicated that activation of the aliphatic C–H bonds of the linker by the putative nitride provided the source of the N–H bonds in **66**. This hypothesis was further supported by the isolation of a ligand C–H activation product, **67**, following thermolysis of **65** in the solid state at 60 °C. This product results from the net insertion of a nitrogen atom into a C–H bond on the central methylene group of the alkyl linker.

The reactivity of the putative dicobalt bridging nitride appeared to be altered when a macrocycle with a shorter alkyl linker was employed. Use of the two-carbon bridged ligand $^2PDI_2$ led to the formation of two isolable products following azide decomposition: a μ-NH_2 species, **70**, and a product with a bridging phosphinimide unit, **69** (Scheme 17). P–N bond formation via attack of a phosphine on an electrophilic nitride is a well-known reaction in late-metal, terminal nitride chemistry,[155] but it had not previously been demonstrated at a bridging nitride. Differing product distributions and reaction dependencies (e.g. on the concentration of added PMe_3) between the $^2PDI_2$- and $^3PDI_2$-supported nitrides indicate that the geometric constraints of the macrocycle are imparting reaction selectivity that may be exploited in more well-behaved systems.

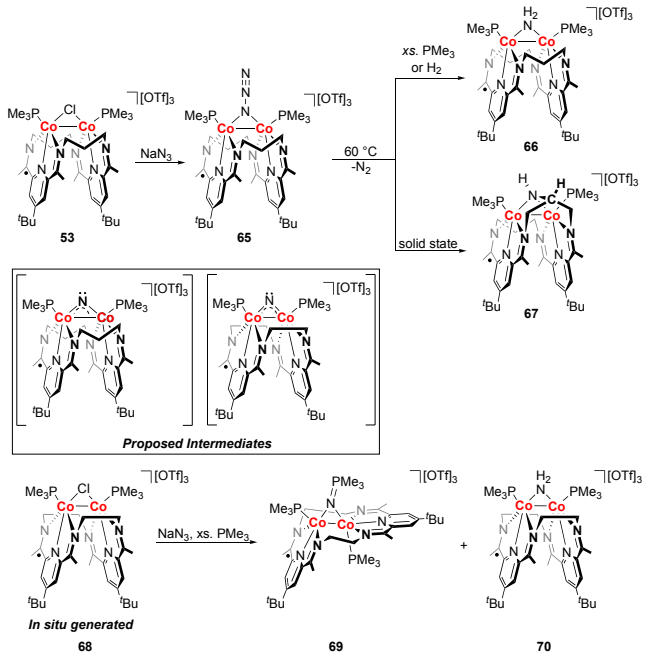

Scheme 17 Difference in reactivity of the putative nitride formed with the $^3PDI_2$ ligand and $^2PDI_2$ ligand.

Conclusions

The examples covered in the Feature Article were intended to demonstrate how judicious ligand design can be used to facilitate *cooperative* small molecule activation by multimetallic complexes. By creating ligand frameworks specifically designed to house multiple metal centers, entirely new methods for small molecule activation and catalysis are being discovered. From dinuclear oxidative addition and reductive elimination to cooperative cycloaddition chemistry, traditional inorganic and organometallic reactivity is being cast in a new light as chemists gain control over the coordination environment of multinuclear metal complexes.

It is clear from the wide variety of ligands designed to support multimetallic centers that control of the intermetallic distance plays a significant role in the mode of multinuclear small molecule activation. When the intermetallic distances are short, substrates tend to bind in a μ-η^1:η^1, μ-η^1:η^2, or less commonly, μ-η^2:η^2 fashion that allows for retention of the M–M bonds. With larger intermetallic distances, substrates more commonly access M-X-Y-M moieties (μ-κ^1:κ^1) with no M–M

bonding interaction. This comparison highlights how even minor changes to the ligand architecture can have an outsized impact on the system's mode of reactivity. Other design considerations naturally include the donor choice and the geometry of the primary coordination sphere about each metal center, but an additional element that has arisen in several of these early ligand designs is the inclusion of redox-active ligands within the multimetallic support. The interplay of these elements with the compact valence manifold of M–M bonded cores is highly system dependent but offers a way to increase the electronic flexibility in a way that should be useful for catalytic applications.

Work in our group has taken into consideration both this ligand redox-activity and tunable intermetallic distances when pursuing bimetallic chemistry. The $^{n}PDI_2$ ligand scaffold is able to hold bimetallic cores within a range of intermetallic distances, owing, in part, to the unique ability of the $^{n}PDI_2$ class of ligands to adopt various geometries (stair-step, folded, arched) and oxidation states in response to the requirements of the cluster core. The constrained geometry imparted by the macrocycle appears, however, to prevent access to thermodynamic sinks, as evidenced by the various small molecule binding motifs described above that are unique to the $^{n}PDI_2$-supported complexes. For example, the stair-step ligand geometry was able to stabilize the μ-N in **62**, but the ligand folded to accommodate the formation of sp^3-hybridized bridging amides following PCET and E–H insertion reactions. Similarly, the arched ligand geometries in ^{PR3}**58** and **60** lead to unique μ-N_2 and μ-CN geometries that promote mixing of the metal's d_σ manifold with the substrate's π* system. This strategy of introducing limited geometric flexibility appears to add a new dimension to the development of ligands that are capable of supporting multinuclear complexes for small molecule activation chemistry.

In conclusion, ligand design to support multimetallic complexes that undergo cooperative, small molecule activation is a robust and active field of research. The reaction pathways available to these systems are highly dependent on intermetallic distances, the redox activity of the ligand, and the coordination environment of the metal centers. Despite these developments, the use of ligands that contain redox-active elements is underexplored, and the use of those with limited geometrical flexibility is virtually unknown. However, our results indicate that the combination of these features offers a new horizon in the discovery of novel reaction pathways and catalysts. Future work will need to be done to improve the connections between these variables and the multinuclear sites of metalloenzymes and metallic surfaces. In particular, the effects of geometric constraints on the electronic structures and reactivity profiles of small molecules will be of interest. We further anticipate that future challenges in this field will include both the rational design of supported complexes that feature heterometallic centers and designs that enable precise control over the geometries of the complexes that are formed.

Conflicts of interest

There are no conflicts to declare.

Acknowledgements

We thank the National Science Foundation (CHE-1945265), the National Institute of General Medical Sciences of the National Institutes of Health (R35GM128794), the Vagelos Institute for Energy Science and Technology (Graduate Research Fellowship to TL), and the University of Pennsylvania for financial support.

Notes and references

1. N. Stucke, B. M. Flöser, T. Weyrich and F. Tuczek, *Eur. J. Inorg. Chem.*, 2018, **2018**, 1337-1355.
2. Q. Zeng, F. W. Lewis, L. M. Harwood and F. Hartl, *Coord. Chem. Rev.*, 2015, **304-305**, 88-101.
3. S. Itoh, *Acc. Chem. Res.*, 2015, **48**, 2066-2074.
4. D. G. H. Hetterscheid and J. N. H. Reek, *Angew. Chem. Int. Ed.*, 2012, **51**, 9740-9747.
5. W. Nam, Y.-M. Lee and S. Fukuzumi, *Acc. Chem. Res.*, 2014, **47**, 1146-1154.
6. R. Drozdzak, B. Allaert, N. Ledoux, I. Dragutan, V. Dragutan and F. Verpoort, *Coord. Chem. Rev.*, 2005, **249**, 3055-3074.
7. J. Wei and E. Iglesia, *J. Catal.*, 2004, **224**, 370-383.
8. R. Schlögl, in *Handbook of Heterogeneous Catalysis*, eds. G. Ertl, H. Knözinger, F. Schüth and J. Weitkamp, Wiley-VCH Verlag GmbH & Co. KGaA, Weinheim, 2008, ch. 12, pp. 2501-2575.
9. F. Kapteijn, J. Rodriguez-Mirasol and J. A. Moulijn, *Appl. Catal. B*, 1996, **9**, 25-64.
10. Z. Gholami, Z. Tišler and V. Rubáš, *Catal. Rev.*, 2020, 1-84.
11. A. Sekretaryova, S. M. Jones and E. I. Solomon, *J. Am. Chem. Soc.*, 2019, **141**, 11304-11314.
12. E. I. Solomon, *Inorg. Chem.*, 2016, **55**, 6364-6375.
13. B. M. Hoffman, D. Lukoyanov, Z.-Y. Yang, D. R. Dean and L. C. Seefeldt, *Chem. Rev.*, 2014, **114**, 4041-4062.
14. W. Kang, C. C. Lee, A. J. Jasniewski, M. W. Ribbe and Y. Hu, *Science*, 2020, **368**, 1381-1385.
15. P. Kalck, *Homo- and Heterobimetallic Complexes in Catalysis: Cooperative Catalysis*, Springer International Publishing AG Switzerland, Switzerland, 2016.
16. B. Chatterjee, W.-C. Chang, S. Jena and C. Werlé, *ACS Catal.*, 2020, **10**, 14024-14055.
17. E. L. Muetterties, *Science*, 1977, **196**, 839-848.
18. A. M. Bradshaw, *Surf. Sci.*, 1995, **331-333**, 978-988.
19. E. L. Muetterties, T. N. Rhodin, E. Band, C. F. Brucker and W. R. Pretzer, *Chem. Rev.*, 1979, **79**, 91-137.
20. D. M. P. Mingos, *J. Clust. Sci.*, 1992, **3**, 397-409.
21. P. J. Dyson, *Coord. Chem. Rev.*, 2004, **248**, 2443-2458.
22. J. Zwart and R. Snel, *J. Mol. Catal.*, 1985, **30**, 305-352.
23. T. A. Pakkanen, J. Pursiainen, T. Venäläinen and T. T. Pakkanen, *J. Organomet. Chem.*, 1989, **372**, 129-139.
24. T. Shima, Y. Luo, T. Stewart, R. Bau, G. J. McIntyre, S. A. Mason and Z. Hou, *Nat. Chem.*, 2011, **3**, 814-820.
25. A. M. Baranger, T. A. Hanna and R. G. Bergman, *J. Am. Chem. Soc.*, 1995, **117**, 10041-10046.
26. P. Buchwalter, J. Rosé and P. Braunstein, *Chem. Rev.*, 2015, **115**, 28-126.
27. L. H. Gade, *Angew. Chem. Int. Ed.*, 2000, **39**, 2658-2678.
28. M. Knorr and I. Jourdain, *Coord. Chem. Rev.*, 2017, **350**, 217-247.
29. N. Wheatley and P. Kalck, *Chem. Rev.*, 1999, **99**, 3379-3420.
30. Y. Ohki, N. Matsuura, T. Marumoto, H. Kawaguchi and K. Tatsumi, *J. Am. Chem. Soc.*, 2003, **125**, 7978-7988.
31. T. J. Mazzacano and N. P. Mankad, *J. Am. Chem. Soc.*, 2013, **135**, 17258-17261.

32. M. M. Shoshani and S. A. Johnson, *Nat. Chem.*, 2017, **9**, 1282-1285.
33. M. Aufiero, T. Sperger, A. S.–K. Tsang and F. Schoenebeck, *Angew. Chem. Int. Ed.*, 2015, **54**, 10322-10326.
34. B. G. Cooper, J. W. Napoline and C. M. Thomas, *Catal. Rev.*, 2012, **54**, 1-40.
35. A. Cirri, H. Morales Hernández, C. Kmiotek and C. J. Johnson, *Angew. Chem. Int. Ed.*, 2019, **58**, 13818-13822.
36. G. Liu, V. Chauhan, A. P. Aydt, S. M. Ciborowski, A. Pinkard, Z. Zhu, X. Roy, S. N. Khanna and K. H. Bowen, *J. Phys. Chem. C*, 2019, **123**, 25121-25127.
37. R. C. Cammarota, L. J. Clouston and C. C. Lu, *Coord. Chem. Rev.*, 2017, **334**, 100-111.
38. J. T. Moore and C. C. Lu, *J. Am. Chem. Soc.*, 2020, **142**, 11641-11646.
39. J. P. Krogman and C. M. Thomas, *Chem. Commun.*, 2014, **50**, 5115-5127.
40. H. Zhang, G. P. Hatzis, C. E. Moore, D. A. Dickie, M. W. Bezpalko, B. M. Foxman and C. M. Thomas, *J. Am. Chem. Soc.*, 2019, **141**, 9516-9520.
41. K. P. Kornecki, J. F. Berry, D. C. Powers and T. Ritter, in *Prog. Inorg. Chem.*, ed. K. D. Karlin, John Wiley & Sons, Inc., Hoboken, New Jersey, 2014, vol. 58, ch. 4, pp. 225-302.
42. J. E. McGrady, in *Comprehensive Inorganic Chemistry II (Second Edition)*, eds. J. Reedijk and K. Poeppelmeier, Elsevier, Amsterdam, 2013, vol. 9, pp. 321-340.
43. J. Hansen and H. M. L. Davies, *Coord. Chem. Rev.*, 2008, **252**, 545-555.
44. K. Liao, T. C. Pickel, V. Boyarskikh, J. Bacsa, D. G. Musaev and H. M. L. Davies, *Nature*, 2017, **551**, 609-613.
45. C. Werlé, R. Goddard, P. Philipps, C. Farès and A. Fürstner, *J. Am. Chem. Soc.*, 2016, **138**, 3797-3805.
46. K. P. Kornecki, J. F. Briones, V. Boyarskikh, F. Fullilove, J. Autschbach, K. E. Schrote, K. M. Lancaster, H. M. L. Davies and J. F. Berry, *Science*, 2013, **342**, 351-354.
47. R. C. Cammarota, J. Xie, S. A. Burgess, M. V. Vollmer, K. D. Vogiatzis, J. Ye, J. C. Linehan, A. M. Appel, C. Hoffmann, X. Wang, V. G. Young, Jr. and C. C. Lu, *Chem. Sci.*, 2019, **10**, 7029-7042.
48. J. A. Hlina, J. R. Pankhurst, N. Kaltsoyannis and P. L. Arnold, *J. Am. Chem. Soc.*, 2016, **138**, 3333-3345.
49. B. Battistella and K. Ray, *Coord. Chem. Rev.*, 2020, **408**, 1-13.
50. T. Glaser, *Coord. Chem. Rev.*, 2019, **380**, 353-377.
51. V. Lozan, C. Loose, J. Kortus and B. Kersting, *Coord. Chem. Rev.*, 2009, **253**, 2244-2260.
52. A. Neves, M. Lanznaster, A. J. Bortoluzzi, R. A. Peralta, A. Casellato, E. E. Castellano, P. Herrald, M. J. Riley and G. Schenk, *J. Am. Chem. Soc.*, 2007, **129**, 7486-7487.
53. A. C. Deacy, A. F. R. Kilpatrick, A. Regoutz and C. K. Williams, *Nat. Chem.*, 2020, **12**, 372-380.
54. H.-C. Chiu, A. Koley, P. L. Dunn, R. J. Hue and I. A. Tonks, *Dalton Trans.*, 2017, **46**, 5513-5517.
55. G. Trott, J. A. Garden and C. K. Williams, *Chem. Sci.*, 2019, **10**, 4618-4627.
56. E. Askarizadeh, S. B. Yaghoob, D. M. Boghaei, A. M. Z. Slawin and J. B. Love, *Chem. Commun.*, 2010, **46**, 710-712.
57. J. Park and S. Hong, *Chem. Soc. Rev.*, 2012, **41**, 6931-6943.
58. D.-H. Manz, P.-C. Duan, S. Dechert, S. Demeshko, R. Oswald, M. John, R. A. Mata and F. Meyer, *J. Am. Chem. Soc.*, 2017, **139**, 16720-16731.
59. P.-C. Duan, D.-H. Manz, S. Dechert, S. Demeshko and F. Meyer, *J. Am. Chem. Soc.*, 2018, **140**, 4929-4939.
60. E. Ferretti, S. Dechert and F. Meyer, *Inorg. Chem.*, 2019, **58**, 5154-5162.
61. E. Ferretti, S. Dechert, S. Demeshko, M. C. Holthausen and F. Meyer, *Angew. Chem. Int. Ed.*, 2019, **58**, 1705-1709.
62. T. Hayashi, J. D. Caranto, D. A. Wampler, D. M. Kurtz and P. Moënne-Loccoz, *Biochemistry*, 2010, **49**, 7040-7049.
63. C. Van Stappen and N. Lehnert, *Inorg. Chem.*, 2018, **57**, 4252-4269.
64. A. M. Wright, H. T. Zaman, G. Wu and T. W. Hayton, *Inorg. Chem.*, 2014, **53**, 3108-3116.
65. R. B. Ferreira and L. J. Murray, *Acc. Chem. Res.*, 2019, **52**, 447-455.
66. M. C. Eaton, B. J. Knight, V. J. Catalano and L. J. Murray, *Eur. J. Inorg. Chem.*, 2020, **2020**, 1519-1524.
67. K. J. Anderton, D. M. Ermert, P. A. Quintero, M. W. Turvey, M. S. Fataftah, K. A. Abboud, M. W. Meisel, E. Čižmár and L. J. Murray, *Inorg. Chem.*, 2017, **56**, 12012-12022.
68. Y. Lee, K. J. Anderton, F. T. Sloane, D. M. Ermert, K. A. Abboud, R. García-Serres and L. J. Murray, *J. Am. Chem. Soc.*, 2015, **137**, 10610-10617.
69. L. J. Murray, W. W. Weare, J. Shearer, A. D. Mitchell and K. A. Abboud, *J. Am. Chem. Soc.*, 2014, **136**, 13502-13505.
70. G. N. Di Francesco, A. Gaillard, I. Ghiviriga, K. A. Abboud and L. J. Murray, *Inorg. Chem.*, 2014, **53**, 4647-4654.
71. B. J. Cook, G. N. Di Francesco, R. B. Ferreira, J. T. Lukens, K. E. Silberstein, B. C. Keegan, V. J. Catalano, K. M. Lancaster, J. Shearer and L. J. Murray, *Inorg. Chem.*, 2018, **57**, 11382-11392.
72. B. J. Cook, G. N. Di Francesco, M. T. Kieber-Emmons and L. J. Murray, *Inorg. Chem.*, 2018, **57**, 11361-11368.
73. Y. Lee, F. T. Sloane, G. Blondin, K. A. Abboud, R. García-Serres and L. J. Murray, *Angew. Chem. Int. Ed.*, 2015, **54**, 1499-1503.
74. R. B. Ferreira, B. J. Cook, B. J. Knight, V. J. Catalano, R. García-Serres and L. J. Murray, *ACS Catal.*, 2018, **8**, 7208-7212.
75. M. M. Rodriguez, E. Bill, W. W. Brennessel and P. L. Holland, *Science*, 2011, **334**, 780-783.
76. D. M. Ermert, J. B. Gordon, K. A. Abboud and L. J. Murray, *Inorg. Chem.*, 2015, **54**, 9282-9289.
77. T. M. Powers, A. R. Fout, S.-L. Zheng and T. A. Betley, *J. Am. Chem. Soc.*, 2011, **133**, 3336-3338.
78. T. M. Powers and T. A. Betley, *J. Am. Chem. Soc.*, 2013, **135**, 12289-12296.
79. H. Zhang, G. P. Hatzis, D. A. Dickie, C. E. Moore and C. M. Thomas, *Chem. Sci.*, 2020, **11**, 10729-10736.
80. G. Culcu, D. A. Iovan, J. P. Krogman, M. J. T. Wilding, M. W. Bezpalko, B. M. Foxman and C. M. Thomas, *J. Am. Chem. Soc.*, 2017, **139**, 9627-9636.
81. C. M. Thomas, J. W. Napoline, G. T. Rowe and B. M. Foxman, *Chem. Commun.*, 2010, **46**, 5790-5792.
82. J. W. Beattie, C. Wang, H. Zhang, J. P. Krogman, B. M. Foxman and C. M. Thomas, *Dalton Trans.*, 2020, **49**, 2407-2411.
83. J. W. Napoline, J. P. Krogman, R. Shi, S. Kuppuswamy, M. W. Bezpalko, B. M. Foxman and C. M. Thomas, *Eur. J. Inorg. Chem.*, 2013, **2013**, 3874-3882.
84. S. L. Marquard, M. W. Bezpalko, B. M. Foxman and C. M. Thomas, *J. Am. Chem. Soc.*, 2013, **135**, 6018-6021.
85. S. L. Marquard, M. W. Bezpalko, B. M. Foxman and C. M. Thomas, *Organometallics*, 2014, **33**, 2071-2079.
86. J. P. Krogman, B. M. Foxman and C. M. Thomas, *J. Am. Chem. Soc.*, 2011, **133**, 14582-14585.
87. B. Wu, K. M. Gramigna, M. W. Bezpalko, B. M. Foxman and C. M. Thomas, *Inorg. Chem.*, 2015, **54**, 10909-10917.

88. B. Wu, M. W. Bezpalko, B. M. Foxman and C. M. Thomas, *Chem. Sci.*, 2015, **6**, 2044-2049.
89. K. M. Gramigna, D. A. Dickie, B. M. Foxman and C. M. Thomas, *ACS Catal.*, 2019, **9**, 3153-3164.
90. O. R. Luca and R. H. Crabtree, *Chem. Soc. Rev.*, 2013, **42**, 1440-1459.
91. W. Kaim and B. Schwederski, *Coord. Chem. Rev.*, 2010, **254**, 1580-1588.
92. S. D. Walker, T. E. Barder, J. R. Martinelli and S. L. Buchwald, *Angew. Chem. Int. Ed.*, 2004, **43**, 1871-1876.
93. J. Yin, M. P. Rainka, X.-X. Zhang and S. L. Buchwald, *J. Am. Chem. Soc.*, 2002, **124**, 1162-1163.
94. A. Velian, S. Lin, A. J. M. Miller, M. W. Day and T. Agapie, *J. Am. Chem. Soc.*, 2010, **132**, 6296-6297.
95. K. T. Horak, A. Velian, M. W. Day and T. Agapie, *Chem. Commun.*, 2014, **50**, 4427-4429.
96. J. T. Henthorn, S. Lin and T. Agapie, *J. Am. Chem. Soc.*, 2015, **137**, 1458-1464.
97. J. T. Henthorn and T. Agapie, *Inorg. Chem.*, 2016, **55**, 5337-5342.
98. J. A. Buss, G. A. Edouard, C. Cheng, J. Shi and T. Agapie, *J. Am. Chem. Soc.*, 2014, **136**, 11272-11275.
99. J. K. Bera, N. Sadhukhan and M. Majumdar, *Eur. J. Inorg. Chem.*, 2009, **2009**, 4023-4038.
100. S. Deolka, O. Rivada-Wheelaghan, S. L. Aristizábal, R. R. Fayzullin, S. Pal, K. Nozaki, E. Khaskin and J. R. Khusnutdinova, *Chem. Sci.*, 2020, **11**, 5494-5502.
101. C. N. Brodsky, G. Passard, A. M. Ullman, D. E. Jaramillo, E. D. Bloch, M. Huynh, D. Gygi, C. Costentin and D. G. Nocera, *Dalton Trans.*, 2018, **47**, 11903-11908.
102. B.-C. Tsai, Y.-H. Liu, S.-M. Peng and S.-T. Liu, *Eur. J. Inorg. Chem.*, 2016, **2016**, 2783-2790.
103. C. He and S. J. Lippard, *Inorg. Chem.*, 2001, **40**, 1414-1420.
104. I. Dutta, A. Sarbajna, P. Pandey, S. M. W. Rahaman, K. Singh and J. K. Bera, *Organometallics*, 2016, **35**, 1505-1513.
105. B. Saha, S. M. Wahidur Rahaman, P. Daw, G. Sengupta and J. K. Bera, *Chem. Eur. J.*, 2014, **20**, 6542-6551.
106. I. Dutta, S. De, S. Yadav, R. Mondol and J. K. Bera, *J. Organomet. Chem.*, 2017, **849-850**, 117-124.
107. B.-S. Liao and S.-T. Liu, *Catal. Commun.*, 2013, **32**, 28-31.
108. T. C. Davenport and T. D. Tilley, *Angew. Chem. Int. Ed.*, 2011, **50**, 12205-12208.
109. M. S. Ziegler, D. S. Levine, K. V. Lakshmi and T. D. Tilley, *J. Am. Chem. Soc.*, 2016, **138**, 6484-6491.
110. T. C. Davenport and T. D. Tilley, *Dalton Trans.*, 2015, **44**, 12244-12255.
111. A. Nicolay, M. S. Ziegler, D. W. Small, R. Grünbauer, M. Scheer and T. D. Tilley, *Chem. Sci.*, 2020, **11**, 1607-1616.
112. M. S. Ziegler, K. V. Lakshmi and T. D. Tilley, *J. Am. Chem. Soc.*, 2017, **139**, 5378-5386.
113. E. Kounalis, M. Lutz and D. L. J. Broere, *Chem. Eur. J.*, 2019, **25**, 13280-13284.
114. E. Kounalis, M. Lutz and D. L. J. Broere, *Organometallics*, 2020, **39**, 585-592.
115. Y.-Y. Zhou, D. R. Hartline, T. J. Steiman, P. E. Fanwick and C. Uyeda, *Inorg. Chem.*, 2014, **53**, 11770-11777.
116. M. J. Behlen, Y.-Y. Zhou, T. J. Steiman, S. Pal, D. R. Hartline, M. Zeller and C. Uyeda, *Dalton Trans.*, 2017, **46**, 5493-5497.
117. Y.-Y. Zhou and C. Uyeda, *Angew. Chem. Int. Ed.*, 2016, **55**, 3171-3175.
118. S. Pal, Y.-Y. Zhou and C. Uyeda, *J. Am. Chem. Soc.*, 2017, **139**, 11686-11689.
119. M. J. Behlen and C. Uyeda, *J. Am. Chem. Soc.*, 2020, **142**, 17294-17300.
120. Y.-Y. Zhou and C. Uyeda, *Science*, 2019, **363**, 857-862.
121. T. J. Steiman and C. Uyeda, *J. Am. Chem. Soc.*, 2015, **137**, 6104-6110.
122. I. G. Powers, C. Kiattisewee, K. C. Mullane, E. J. Schelter and C. Uyeda, *Chem. Eur. J.*, 2017, **23**, 7694-7697.
123. D. R. Hartline, M. Zeller and C. Uyeda, *J. Am. Chem. Soc.*, 2017, **139**, 13672-13675.
124. H. R. Rounds, M. Zeller and C. Uyeda, *Organometallics*, 2018, **37**, 545-550.
125. I. G. Powers, J. M. Andjaba, X. Luo, J. Mei and C. Uyeda, *J. Am. Chem. Soc.*, 2018, **140**, 4110-4118.
126. A. K. Maity, M. Zeller and C. Uyeda, *Organometallics*, 2018, **37**, 2437-2441.
127. I. G. Powers, J. M. Andjaba, M. Zeller and C. Uyeda, *Organometallics*, 2020, **39**, 3794-3801.
128. A. K. Maity, A. E. Kalb, M. Zeller and C. Uyeda, *Angew. Chem. Int. Ed.*, 2020, **60**, 1897-1902.
129. D. R. Hartline, M. Zeller and C. Uyeda, *Angew. Chem. Int. Ed.*, 2016, **55**, 6084-6087.
130. S. Pal and C. Uyeda, *J. Am. Chem. Soc.*, 2015, **137**, 8042-8045.
131. N. E. Schore, in *Organic Reactions*, John Wiley & Sons, Inc., 2004, pp. 1-90.
132. R. J. Baxter, G. R. Knox, J. H. Moir, P. L. Pauson and M. D. Spicer, *Organometallics*, 1999, **18**, 206-214.
133. S. C. Bart, K. Chłopek, E. Bill, M. W. Bouwkamp, E. Lobkovsky, F. Neese, K. Wieghardt and P. J. Chirik, *J. Am. Chem. Soc.*, 2006, **128**, 13901-13912.
134. C. Römelt, T. Weyhermüller and K. Wieghardt, *Coord. Chem. Rev.*, 2019, **380**, 287-317.
135. J. Dou, Z. Sun, A. A. Opalade, N. Wang, W. Fu and F. Tao, *Chem. Soc. Rev.*, 2017, **46**, 2001-2027.
136. M. G. B. Drew, J. Nelson, F. Esho, V. McKee and S. M. Nelson, *J. Chem. Soc., Dalton Trans.*, 1982, 1837-1843.
137. C. Harding, D. McDowell, J. Nelson, S. Raghunathan, C. Stevenson, M. G. B. Drew and P. C. Yates, *J. Chem. Soc., Dalton Trans.*, 1990, 2521-2533.
138. M. G. B. Drew, M. McCann and S. M. Nelson, *J. Chem. Soc., Chem. Commun.*, 1979, 481-482.
139. M. G. B. Drew, M. McCann and S. M. Nelson, *J. Chem. Soc., Dalton Trans.*, 1981, 1868-1878.
140. B. P. Murphy, J. Nelson, S. M. Nelson, M. G. B. Drew and P. C. Yates, *J. Chem. Soc., Dalton Trans.*, 1987, 123-127.
141. S. Zhang, Q. Wang, L. M. Thierer, A. B. Weberg, M. R. Gau, P. J. Carroll and N. C. Tomson, *Inorg. Chem.*, 2019, **58**, 12234-12244.
142. Q. Wang, S. Zhang, P. Cui, A. B. Weberg, L. M. Thierer, B. C. Manor, M. R. Gau, P. J. Carroll and N. C. Tomson, *Inorg. Chem.*, 2020, **59**, 4200-4214.
143. F. A. Cotton, *Acc. Chem. Res.*, 1978, **11**, 225-232.
144. L. Pauling, *J. Am. Chem. Soc.*, 1947, **69**, 542-553.
145. T. Liu, M. R. Gau and N. C. Tomson, *J. Am. Chem. Soc.*, 2020, **142**, 8142-8146.
146. K. Grubel, W. W. Brennessel, B. Q. Mercado and P. L. Holland, *J. Am. Chem. Soc.*, 2014, **136**, 16807-16816.
147. D. Sorsche, M. E. Miehlich, K. Searles, G. Gouget, E. M. Zolnhofer, S. Fortier, C.-H. Chen, M. Gau, P. J. Carroll, C. B. Murray, K. G. Caulton, M. M. Khusniyarov, K. Meyer and D. J. Mindiola, *J. Am. Chem. Soc.*, 2020, **142**, 8147-8159.
148. J. J. Mortensen, L. B. Hansen, B. Hammer and J. K. Nørskov, *J. Catal.*, 1999, **182**, 479-488.

149. A. Z. Spentzos, M. R. Gau, P. J. Carroll and N. C. Tomson, *Chem. Commun.*, 2020, **56**, 9675-9678.
150. S. Zhang, P. Cui, T. Liu, Q. Wang, T. J. Longo, L. M. Thierer, B. C. Manor, M. R. Gau, P. J. Carroll, G. C. Papaefthymiou and N. C. Tomson, *Angew. Chem. Int. Ed.*, 2020, **59**, 15215-15219.
151. S. D. Brown and J. C. Peters, *J. Am. Chem. Soc.*, 2005, **127**, 1913-1923.
152. E. R. King, E. T. Hennessy and T. A. Betley, *J. Am. Chem. Soc.*, 2011, **133**, 4917-4923.
153. P. Cui, Q. Wang, S. P. McCollom, B. C. Manor, P. J. Carroll and N. C. Tomson, *Angew. Chem. Int. Ed.*, 2017, **56**, 15979-15983.
154. D. Sengupta, C. Sandoval-Pauker, E. Schueller, A. M. Encerrado-Manriquez, A. Metta-Magaña, W.-Y. Lee, R. Seshadri, B. Pinter and S. Fortier, *J. Am. Chem. Soc.*, 2020, **142**, 8233-8242.
155. J. M. Smith, in *Prog. Inorg. Chem.*, ed. K. D. Karlin, John Wiley & Sons, Inc., Hoboken, New Jersey, 2014, vol. 58, ch. 6, pp. 417-470.

Biographical information

Qiuran Wang was born in Beijing, China. He worked with Prof. Fuqiang Huang on the solvothermal and hydrothermal syntheses of tertiary chalcogenide materials in Peking University and graduated with a B.S. in Chemistry in 2013. After that, he studied Materials Science and Engineering at the University of Pennsylvania, where he obtained a Master's degree in 2015. He stayed at the same school, turned into a Chemistry Ph.D. student, and joined the Tomson group in 2016 and started conducting research on organometallic chemistry. He is currently working on multimetallic complexes supported by redox-active macrocyclic ligands.

Sam Brooks received a B.S. in Chemistry from Elizabethtown College in 2016. He is currently pursuing a Ph.D. under Neil Tomson at the University of Pennsylvania. His research focuses on evaluating the reactivity of dicopper *bis*(pyridyldiimine) macrocycles. He is also pursuing the development of new *bis*(pyridyldiimine) macrocyclic ligands for use in invoking new reactivity in bimetallic, late first-row transition metal complexes.

Tianchang Liu was born in Qingdao, China. He obtained a B.S. from Nankai University in 2018. At Nankai, he worked with Prof. Mengchun Ye on internal olefin functionalization catalyzed by Ni–Al bimetallics, and in 2017 he worked with Prof. Paula Diaconescu at UCLA on yttrium-catalyzed ring-opening polymerization of cyclic esters. In 2018, He came to UPenn as a Ph.D. student in Chemistry and joined the Tomson group. He is currently working with nitrogenous iron complexes as molecular mimics to key intermediates in industrial and biological nitrogen fixation.

Neil Tomson received a B.A. in Chemistry in 2004 from Grinnell College (Prof. T. Andrew Mobley) and a Ph.D. in 2009 from the University of California, Berkeley (Profs. John Arnold and Robert G. Bergman). He held post-doctoral positions at the Max Planck Institute for Bioinorganic Chemistry (now Chemical Energy Conversion; Prof. Dr. Karl Wieghardt) and Los Alamos National Laboratory (Prof. James M. Boncella) before joining the faculty at the University of Pennsylvania in 2015. His awards include Glenn T. Seaborg and Director's Post-doctoral Fellowships at LANL and a 2019 NSF CAREER Award.